Pergamon

Cement and Concrete Research, Vol. 27, No. 8, pp. 1167–1177, 1997

0008-8846/97 $17.00 + .00

PII S0008-8846(97)00120-8

DISTRIBUTION OF IRON AMONG FERRITE HYDRATES

Anna Emanuelson and Staffan Hansen
National Center for HREM, Inorganic Chemistry 2, Chemical Center, Lund University
P.O. Box 124, SE-221 00 Lund, Sweden

(Refereed)
(Received May 2, 1997; in final form June 30, 1997)

ABSTRACT

The hydration products of Ca_2AlFeO_5 pastes at 20°C were characterized by X-ray powder diffraction, secondary electron imaging and X-ray microanalysis. In pure water, two X-ray amorphous AFm phases, one Al-rich and one Fe-rich, are initially formed. AFm is then replaced by hydrogarnet (Al/Al + Fe ≈ 3/4). In the presence of gypsum, AFt needles are first formed, followed by platy sulphate-AFm (both with Al/Al + Fe ≈ 3/4). With $Ca(OH)_2$ and gypsum, the following was observed (cf. gypsum only): (i) higher Fe content in AFt and AFm, i.e., Al/Al + Fe ≈1/2; (ii) decreased amount of S in AFt; and (iii) a general decrease in the crystal size of AFt and AFm. X-ray amorphous pseudomorphs after ferrite grains were present in all runs. Despite the formation of these $CaFe_4O_7 \cdot xH_2O$ residues, much Fe enters the other products, especially when a base is added. It is proposed that the passivity of the ferrite surface is caused by a compact, X-ray amorphous layer desiccated by crystallizing AFt. © *1997 Elsevier Science Ltd*

Introduction

The hydration of ferrite has been subject to several investigations (1-4). Well known phases are formed, e.g. AFt, AFm and hydrogarnet. It has been reported that iron does not form separate phases in the hydration of ferrite, but remains in the structure of the hydrated compounds, substituting for aluminum (5). Other experiments show that the Fe/Al ratios in the hydrated phase AFt vary, depending on the availability of $Ca(OH)_2$, and that amorphous phases, possibly $Fe_2O_3 \cdot nH_2O$ and $Al_2O_3 \cdot nH_2O$, form simultaneously with AFt (6). The Fe/Al ratio in hydrogarnet varies with that in the anhydrous ferrite, however the hydrogarnet is always poorer in iron than the starting material (7). This implies that except for hydrogarnet, other phases must incorporate the excess iron when ferrite is hydrated. An iron-rich residue of the ferrite has been reported (6-9). It was the purpose of the present investigation to outline the reactions of ferrite, the distribution of iron among the products and the ways in which these are affected by addition of $CaSO_4 \cdot 2H_2O$, $Ca(OH)_2$ and Ca_3SiO_5. We also wish to discuss the nature of the covering layer, formed when $Ca(OH)_2$ or Ca_3SiO_5 is present during the hydration, and the mechanism behind the dormant period caused by this layer.

TABLE 1

Composition (wt%) of Mixtures in Hydration Experiments

sample	ferrite	gypsum	$Ca(OH)_2$	Ca_3SiO_5	quartz
1	60	-	-	-	40
2	60	20	-	-	20
3	60	20	10	-	10
4	60	20	-	10	10

Experimental

Synthetic ferrite, Ca_2AlFeO_5, was prepared from $CaCO_3$ (Merck, p.a.), γ-Al_2O_3 (Merck, puriss. water free) and Fe_2O_3 (Merck, p.a.) at 1350°C. Four samples were prepared according to Table 1 by mixing synthetic ferrite with $CaSO_4 \cdot 2H_2O$ (Merck, p.a.), $Ca(OH)_2$ (Merck, p.a.), Ca_3SiO_5 (prepared from $CaCO_3$ and SiO_2 at 1450°C) and quartz, SiO_2 (3).

The sample (0.5 g) was mixed with 0.5 ml water for 30 seconds, and hydrated for 60 minutes to 4 months, the period depending on reactivity and the products we sought. The hydration was stopped by mixing with acetone (99.5%) for 30 seconds. The sample was vacuum filtered and washed with acetone 4 times and finally dried by vacuum filtering for 8 minutes.

Small amounts of the hydrated samples were mounted on copper stubs covered with a conducting polymer. A thin layer of carbon was then evaporated onto the samples. These stubs were used for EDX analysis in a JSM-840A scanning electron microscope interfaced with a Link AN10000 energy dispersive X-ray microanalysis system. The analyses were made at 20 kV with a probe current of 1 nA. For each phase, about five analyses were performed on different crystals or crystal aggregates. The spectra were gathered in 100 seconds effective-counting-time from an area with an approximate diameter 3 μm. A number of O(2-) was chosen to balance the charges of the cations so that an appropriate cation stoichiometry was achieved. Iron was considered as Fe(3+) in all calculations. Corrections were made for atomic number effects, absorption in the sample and X-ray fluorescence. Small amounts of the samples were also mounted on copper stubs using adhesive tape and then covered by sputtering with a thin layer of gold. These stubs were used to record secondary electron images.

The hydrated samples were mixed with Si powder and mounted on Scotch tape. X-ray powder diffraction films were recorded using a Guinier-Hägg camera (CuKα1 radiation). The phases were identified by comparison with films recorded on reference samples of ferrite, gypsum, ettringite and quartz. The unit cell parameters were determined and refined using the least-squares method and compared with literature data. The reference parameters of AFt and AFm are presented in Table 2.

TABLE 2

Hexagonal Lattice Parameters of AFt and AFm Phases According to the Literature

phase	composition	cement formula	a/Å	c/Å	d_{003}/Å	ref. no.
AFt	$\{Ca_3Al(OH)_6(H_2O)_{12}\}_2(SO_4)_3\cdot 2H_2O$	$C_6A\bar{S}_3H_{32}$	11.22	21.41		11
	$\{Ca_3Al(OH)_6(H_2O)_{12}\}_2(OH)_6\cdot 2H_2O$	C_6AH_{35}	10.90	21.27		12
	$\{Ca_3Al(OH)_6(H_2O)_{12}\}_2(CO_3)_3\cdot 2H_2O$	$C_6A\dot{C}_3H_{32}$	10.86	21.22		12
	$\{Ca_3Fe(OH)_6(H_2O)_{12}\}_2(SO_4)_3\cdot 2H_2O$	$C_6F\bar{S}_3H_{32}$	11.18	22.01		13
AFm	$\{Ca_2Al(OH)_6\}_2(OH)_2\cdot 6H_2O$	C_4AH_{13}			7.94	14
	$\{Ca_2Al(OH)_6\}_2\{Al(OH)_4\}_2\cdot 6H_2O$	C_2AH_8			10.7	15
	$\{Ca_2Al(OH)_6\}_4(OH)_2(CO_3)\cdot 11H_2O$	$C_4A\dot{C}_{0.5}H_{12}$			8.19	16
	$\{Ca_2Al(OH)_6\}_2(SO_4)\cdot 4H_2O$	$C_4A\bar{S}H_{10}$			8.15	17
	$\{Ca_2Al(OH)_6\}_2(SO_4)\cdot 6H_2O$	$C_4A\bar{S}H_{12}$	5.76	26.81	8.94	18
	$\{Ca_2Al(OH)_6\}_2(SO_4)\cdot 8H_2O$	$C_4A\bar{S}H_{14}$	5.75	28.67	9.56	18
	$\{Ca_2Fe(OH)_6\}_2(SO_4)\cdot 6H_2O$	$C_4F\bar{S}H_{12}$	5.89	26.63	8.88	18
	$\{Ca_2Fe(OH)_6\}_2(SO_4)\cdot 8H_2O$	$C_4F\bar{S}H_m$, m>12	5.85		10.21	18

Results

According to XRD analysis, the orthorhombic unit cell parameters of our synthetic ferrite, Ca_2AlFeO_5, were a = 5.5598(7), b = 14.511(2), c = 5.3432(7) Å. This is similar to data reported in the literature, i.e. a = 5.57, b = 14.52, c = 5.35 Å (10).

The estimated standard deviations for the EDX results in Table 3 and 4 are somewhat high, perhaps because the specimens are not ideal, i.e. not a homogenous solid with flat surface. Instead, the individual crystals are often quite small, with the applied vacuum causing water loss and subsequent cracking in some cases. Another cause of the high standard

time	phase	cation composition#	a/Å
60 min	Al-rich AFm	$Ca_{3.6(2)}Al_{2.0(1)}Fe_{0.3(2)}$	*
60 min	Fe-rich AFm	$Ca_{1.7(1)}Al_{0.59(4)}Fe_{1.6(1)}$	*
14 days	hydrogarnet	$Ca_{3.1(2)}Al_{1.3(1)}Fe_{0.6(1)}$	12.593(1)
14 days	Fe-rich ferrite residue	$Ca_{1.0(2)}Al_{0.13(6)}Fe_{3.8(1)}$	*

Estimated standard deviations referring to the last digit are given in parenthesis.

* X-ray amorphous

TABLE 4

Results from EDX and XRD of Ferrite Hydrated for Various Times with Aqueous Solutions Containing Gypsum; Gypsum + $Ca(OH)_2$; and Gypsum + Ca_3SiO_5

additive	time	phase	cation composition#	a/Å	c/Å
gypsum	240 min	AFt	$Ca_{6.0(2)}Al_{1.6(2)}Fe_{0.6(1)}S_{2.9(2)}$	11.213(6)	21.51(2)
	14 days	sulphate-AFm	$Ca_{4.1(2)}Al_{1.5(1)}Fe_{0.4(1)}S_{0.99(8)}$	5.7710(3)	26.674(5)
	240 min	Fe-rich ferrite residue	$Ca_{1.15(8)}Al_{0.08(4)}Fe_{3.83(8)}$	*	*
	14 days	Fe-rich ferrite residue	$Ca_{0.99(4)}Al_{0.08(4)}Fe_{3.93(5)}$	*	*
gypsum + $Ca(OH)_2$	14 days	AFt	$Ca_{5.7(6)}Al_{1.10(8)}Fe_{1.3(3)}S_{1.9(1)}$	11.14(2)	21.78(5)
	4 months	sulphate-AFm	$Ca_{3.9(2)}Al_{1.2(2)}Fe_{1.0(2)}S_{0.9(1)}$	5.762(1)	26.782(7)
	4 months	Fe-rich ferrite residue	$Ca_{1.2(2)}Al_{0.12(8)}Fe_{3.8(2)}$	*	*
gypsum + Ca_3SiO_5	28 days	AFt	$Ca_{5.9(3)}Al_{0.7(1)}Fe_{1.2(2)}S_{2.1(1)}$	11.163(3)	21.959(4)

Estimated standard deviations referring to the last digit are given in parenthesis.
* X-ray amorphous

errors may be the compositional variation of a phase within a sample. Nevertheless, the results are of sufficient quality to allow conclusions on stoichiometries and variations in iron content of solids formed in solutions of different alkalinity.

Hydration of Ferrite in Water. When ferrite is hydrated in water, cf Table 3, an aluminum rich and an iron rich phase of AFm type is formed. EDX analysis indicates the compositions to be $\{Ca_2(Al_{0.9}Fe_{0.1})(OH)_6\}_2(OH)_2 \cdot nH_2O$ and $\{Ca_2(Al_{0.3}Fe_{0.7})(OH)_6\}_2\{(Al_{0.3}Fe_{0.7})(OH)_4\}_2 \cdot nH_2O$, respectively. The composition of Al-rich AFm fits with hydroxide-AFm (Table 2), ideally $\{Ca_2Al(OH)_6\}_2(OH)_2 \cdot nH_2O$ and the composition of the Fe-rich AFm fits with an almost fully iron- substituted analogue of aluminate-AFm (Table 2), ideally $\{Ca_2Fe(OH)_6\}_2\{Fe(OH)_4\}_2 \cdot nH_2O$. The Al-rich AFm plates are curved, often in the shape of a rose. The plates of the Fe-rich AFm are smaller and thinner, and thus distinguishable from the Al-rich AFm phase, see Figs. 1(a) and (b). Neither of these two phases gives diffraction lines in the XRD analysis. After a few hours (3) the AFm phases react further and cubic hydrogarnet is formed, see Figs. 1(c) and (d). There are two types of hydrogarnet, one large, about 30 μm across, with 24 faces (icositetrahedron) and one smaller, about 10 μm, with 12 faces (rhombic dodecahedron). Both forms have the composition $Ca_3(Al_{1.4}Fe_{0.6})(OH)_{12}$. The lattice parameter *a* according to XRD is 12.593(1) Å. Schwiete and Iwai (19) reported that the a repeat is 12.55Å and 12.74Å for the $Ca_3Al_2(OH)_{12}$ and $Ca_3Fe_2(OH)_{12}$, respectively. Thus the hydrogarnet formed in our experiments has a low content of iron, which is consistent with the EDX analysis.

An iron rich phase, $Ca(Al_{0.1}Fe_{3.9})O_7 \cdot nH_2O$, is also formed. It is found in two different shapes, one very similar in outer appearance to the iron rich AFm, see Fig. 1(e), and one that is very similar to unhydrated ferrite particles, see Fig. 1(f). In contrast to the other products formed, the latter product exhibits great variations in particle size, comparable with the particles of ferrite. The phase could not be observed by XRD.

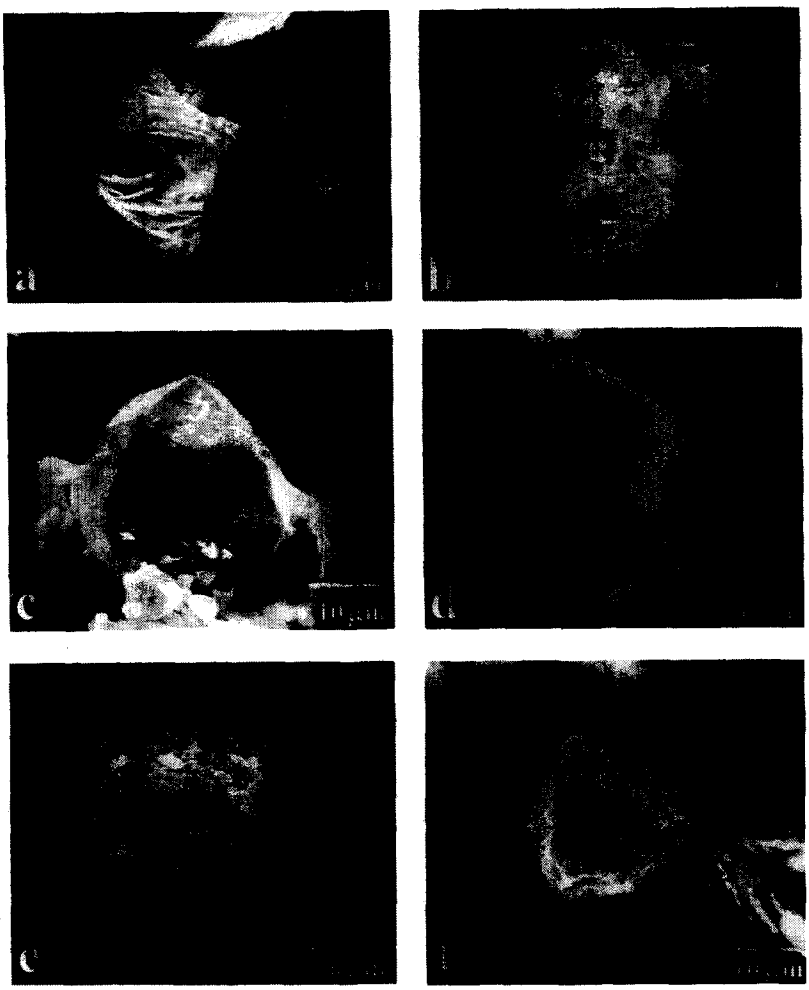

FIG. 1.
(a) Al-rich AFm and (b) Fe-rich AFm formed when ferrite is hydrated for 60 min in pure water. Hydrogarnet formed when ferrite is hydrated for 14 d, (c) icositetrahedra, (d) rhombic dodecahedron. (e) AFm-like and (f) Fe-rich ferrite residue formed when ferrite is hydrated for 14 d.

Hydration of Ferrite in Water with Gypsum. When ferrite is hydrated in water with gypsum, aluminum-rich AFt needles, about 1 μm in length, are formed, see Figs. 2(a) and (c). EDX analysis indicates the composition $\{Ca_3(Al_{0.7}Fe_{0.3})(OH)_6(H_2O)_{12}\}_2(SO_4)_3 \cdot 2H_2O$. XRD analysis also shows that the AFt is aluminum-rich, see Table 2 and 4.

After a few hours (3), aluminum-rich sulphate-AFm is formed from the AFt, see Fig. 2(e). It forms hexagonal plates with the composition $\{Ca_2(Al_{0.8}Fe_{0.2})(OH)_6\}_2(SO_4) \cdot nH_2O$. According to XRD analysis the d_{003} spacing is 8.891 Å, and the phase thus contains n = 6 water, see Table 2 and 4. The *a* parameter indicates that it is close to being iron-free. Two reflections in addition, give d_{003} = 8.24Å, most likely corresponding to a sulphate-AFm with n = 4 water, or a carbonate/hydroxide-AFm, see Table 2. The iron rich phase,

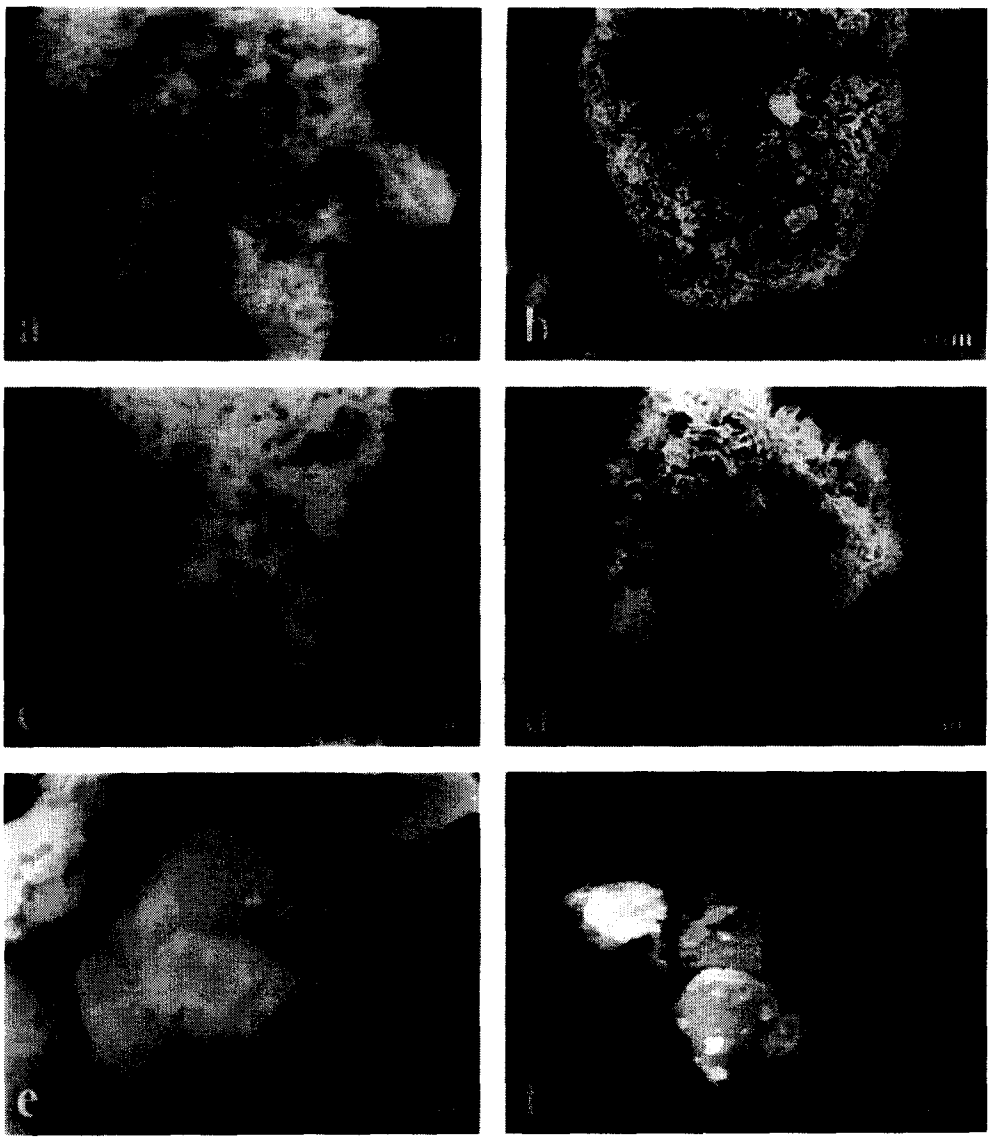

FIG. 2.
AFt-needles formed when ferrite is hydrated with (a) gypsum, 5 min; (b) gypsum + $Ca(OH)_2$, 5 min; (c) gypsum, 240 min; (d) gypsum + $Ca(OH)_2$, 14 days. Sulphate-AFm plates formed when ferrite is hydrated with (e) gypsum, 14 days; (f) gypsum + $Ca(OH)_2$, 4 months.

$Ca(Al_{0.1}Fe_{3.9})O_7 \cdot nH_2O$, was again found, but now only in the shape similar to the unhydrated ferrite particles.

Hydration of Ferrite in Water with Gypsum and $Ca(OH)_2/Ca_3SiO_5$. When ferrite is hydrated in water with gypsum and $Ca(OH)_2$, AFt with approximately equal amounts of iron and aluminum is formed, $\{Ca_3(Al_{0.5}Fe_{0.5})(OH)_6(H_2O)_{12}\}_2(SO_4)_2X \cdot 2H_2O$, X = $(OH)_2^{2-}$ or CO_3^{2-},

see Figs. 2(b) and (d). Except for the low content of aluminum, this compound also has a low content of sulphate. This could be explained by the substitution of interlayer sulphate ions by hydroxide or carbonate ions. XRD analysis shows that the AFt has a smaller *a* repeat and a larger *c* repeat compared to Al-AFt with no anion substitution, cf Table 2 and 4. This could be due to simultaneous substitution of sulphate by hydroxide/carbonate, and aluminum by iron. The AFt crystals are smaller and less well defined compared to the corresponding AFt formed when ferrite is hydrated in the absence of $Ca(OH)_2$.

After a few months (3) the AFt forms sulphate-AFm, with approximately equal amounts of iron and aluminum, $\{Ca_2(Al_{0.5}Fe_{0.5})(OH)_6\}_2(SO_4) \cdot nH_2O$, Fig. 2(f). The AFm crystals are also smaller than the corresponding ones formed in the absence of $Ca(OH)_2$. In the XRD analysis we found that the AFm has $d_{003} = 8.927$ Å, and thus n = 6 water, cf Table 2 and 4. In contrast to the results from EDX, the AFm would appear to be close to iron-free according to its *a* parameter. Two additional basal reflections gave $d_{003} = 9.49$Å and might correspond to an AFm with n = 8 water. However, according to Kuzel (18), this AFm phase only forms with a relative humidity of more than 90%, which is not the case in our experiment unless it corresponds to a storage artefact. We also find the iron-rich phase, $Ca(Al_{0.1}Fe_{3.9})O_7 \cdot nH_2O$, in the shape similar to the unhydrated ferrite particles.

The AFt formed when ferrite is hydrated in the presence of gypsum and Ca_3SiO_5 has the composition $\{Ca_3(Al_{0.4}Fe_{0.6})(OH)_6(H_2O)_{12}\}_2(SO_4)_2X \cdot 2H_2O$, $X = (OH)_2^{2-}$ or CO_3^{2-}. XRD analysis shows that the AFt again has a small *a* repeat and a large *c* repeat, analogous with AFt formed in the presence of gypsum and $Ca(OH)_2$, cf Table 2 and 4.

Colors of Ferrite and its Hydrates. The unreacted samples were olive green, due to their content of ferrite. When the ferrite is hydrated in pure water, the sample first becomes peach-coloured due to the formation of AFm phases. As the AFm phases react further to form hydrogarnet, the sample turns rust red. When ferrite is hydrated in the presence of gypsum (and $Ca(OH)_2/Ca_3SiO_5$), white AFt is formed. Samples with AFt as the major phase thus have a greyish appearance. As the AFt reacts to form AFm, the sample turns peach-colored. In all samples, dark reddish-brown grains of the Fe-rich ferrite residue can be seen in the light microscope, the brown grains become smaller and more equal in size after longer hydration times.

Discussion

This investigation shows that aluminum is not just simply substituted by iron in the hydrates of ferrite, Ca_2AlFeO_5. Different hydrates incorporate different amounts of iron and some hydrates vary in iron content, depending on the availability of $CaSO_4 \cdot 2H_2O$, $Ca(OH)_2$ and Ca_3SiO_5. Even if the finest fraction of the solids present has been filtered off, mass balances offer a useful check of the analysis results. For simplicity, cement formulas will be used (C = CaO, A = Al_2O_3, F = Fe_2O_3, H = H_2O, $\bar{S}$ = SO_3, $\dot{C}$ = CO_2, cf Table 2).

Sample 1. Hydration of ferrite in pure water (molar ratio $C_4AF/H = 1/50$).

$$5C_4AF + (63 + 2x)H \rightarrow 4C_4AH_{13} + C_2FH_8 + AH_3 + 2CF_2H_x \quad [1]$$

$$4C_4AH_{13} + C_2FH_8 + AH_3 \rightarrow 6C_3A_{5/6}F_{1/6}H_6 + 27H \quad [2]$$

C_4AH_{13}, C_2FH_8 and CF_2H_x have been observed in SEM, but not in XRD. C_2FH_8, is suggested to be an iron analogue of the AFm phase C_2AH_8, with $Fe(OH)_4^-$ as interlayer ions. CF_2H_x appears mainly to be a residue of ferrite, but also of C_2FH_8. Carlson (7) has shown by leaching experiments that when C_4AF is hydrated, Ca^{2+} and Al^{3+} are removed from the outer layers, leaving Fe^{3+} at least momentarily, in the original solid. The residue left contains 0.4 CaO per Fe_2O_3. According to Carlson (7), CaO is absorbed on the Fe_2O_3 rather than chemically combined. Brown (6) and Liang and Nanru (9) observed an XRD-amorphous iron-rich phase. However, these workers did not suggest a ferrite residue, but rather a FH_x-gel in association with CaO. We have observed a variation in particle size and shape, comparable with that of ferrite. It is therefore likely that CF_2H_x is formed by dissolution of Ca and Al components from the original ferrite particles. This has also been observed by Fukuhara et al. (8). AH_3 has not been identified, possibly due to a low content, or its presence in the form of an undefined precipitate which may have passed through the filter in the drying procedure. Hydrogarnet has been detected by SEM and XRD. At 25°C it forms a continuous solid solution between C_3AH_6 and C_3FH_6 (16). The C_3FH_6 content was ~25%, which is consistent with Carlson's (7) observation that hydrogarnet always is poorer in iron than the starting material.

Sample 2. Hydration of ferrite in the presence of gypsum if Al-rich AFt and AFm is approximated by the pure Al form (molar ratio $C_4AF/C\bar{S}H_2/H = 1/1/50$).

$$3C_4AF + 9C\bar{S}H_2 + (86 + x)H \rightarrow 3C_6A\bar{S}_3H_{32} + C_2FH_8 + CF_2H_x \quad [3]$$

$$6C_4AF + 3C_6A\bar{S}_3H_{32} + (28 + 2x)H \rightarrow 9C_4A\bar{S}H_{12} + 2C_2FH_8 + 2CF_2H_x \quad [4]$$

Examination in SEM has not so far revealed the presence of C_2FH_8, but of AFt, sulphate-AFm and CF_2H_x. AFt and sulphate-AFm have also been detected by XRD. AFt forms a solid solution between $C_6A\bar{S}_3H_{32}$ and $C_6F\bar{S}_3H_{32}$ at 24°C, with a probable range of immiscibility between 70-80 mol% $C_6F\bar{S}_3H_{32}$ (20). There are also solid solutions between sulphate-, hydroxide- and carbonate-AFt (12). AFt in our experiments has the ratio $F/(F + A) \approx 0.25$ and SO_4^{2-} as interlayer ions. At 25°C AFm has two ranges of solid solution. $C_4F\bar{S}H_x$ accommodates up to about 50 mol% $C_4A\bar{S}H_x$, and $C_4A\bar{S}H_x$ up to about 10 mol% $C_4F\bar{S}H_x$. An intermediate phase with 25-35 mol% $C_4F\bar{S}H_x$ also exists (18). AFm formed in our experiments probably corresponds to the intermediate phase with ~25 mol% $C_4F\bar{S}H_x$.

Samples 3 and 4. Hydration of ferrite in the presence of gypsum and $Ca(OH)_2$, if it is assumed that a SO_4^{2-}-poor AFt is formed (molar ratio in sample 3: $C_4AF/C\bar{S}H_2/CH/H = 1/1/1/50$).

$$C_4AF + 4C\bar{S}H_2 + 4CH + 56H \rightarrow 2C_6A_{0.5}F_{0.5}\bar{S}_2H_{34} \quad [5]$$

$$C_4AF + 2C_6A_{0.5}F_{0.5}\bar{S}_2H_{34} \rightarrow 4C_4A_{0.5}F_{0.5}\bar{S}H_{12} + 20H \quad [6]$$

Examination in SEM and XRD, revealed the presence of AFt and AFm. The AFt formed has the ratio $F/(F + A) \approx 0.5$, and a third of the interlayer SO_4^{2-}-ions are substituted by OH^- and/or CO_3^{2-}. The AFm formed, contains ~50 mol% $C_4F\bar{S}H_x$, and is an end member of the iron-rich solid solution, containing 50-100% $C_4F\bar{S}H_x$ in $C_4A\bar{S}H_x$. Half of the ferrite cannot react according to [5] and [6], since the reactions are limited by $C\bar{S}H_2$ and CH. The re-

maining ferrite probably reacts with water according to reaction [1]. Examination in SEM of sample 3, after 4 months reaction, revealed the presence of both C_2FH_8 and CF_2H_x, as well as grains of intermediate composition. The phases C_4AH_{13} and AH_3 have not been detected.

Hydration of ferrite in the presence of gypsum and Ca_3SiO_5 (sample 4, molar ratio if it is assumed that each C_3S forms one CH: $C_4AF/C\bar{S}H_2/CH/H = 1/1/0.33/50$), is supposed to be analogous to reactions in gypsum + $Ca(OH)_2$ solution.

Concluding Remarks

According to our reaction scheme, there are considerable differences between reactions in a gypsum solution, and those in a gypsum + $Ca(OH)_2/Ca_3SiO_5$ solution. Hydration of ferrite in a gypsum solution distributes iron and aluminum on different hydrates. Aluminum preferentially enters the AFt phase, $C_6A\bar{S}_3H_{32}$, whereas most of the iron enters the AFm phase C_2FH_8 or stays in the ferrite residue CF_2H_x. When ferrite is hydrated in a gypsum + $Ca(OH)_2/Ca_3SiO_5$ solution, *both* iron and aluminum enter the AFt phase, $C_6A_{0.5}F_{0.5}\bar{S}_2H_{34}$.

It has been shown that gypsum and $Ca(OH)_2$ or Ca_3SiO_5 cause a dormant period during the formation of AFt (3,4), but the mechanism behind this behavior is not fully understood. A covering layer, prohibiting diffusion, is often used as an explanation, but the opinions about the nature of this layer differ (1). However, a necessary condition for the phases forming the layer, is that the products are initial. It is a reasonable assumption that the initial products formed on the ferrite surface will be sulphate-free, even if gypsum is present. In the case of C_3A, amorphous AFm phases are often suggested to form (1). But it has also been shown that even after reaction for only 30 seconds, AFt could be detected by DSC in the hydration of C_4AF with gypsum present (4). In the experiments with gypsum reported here, the initial products, responsible for the covering layer, could be amorphous phases, like AFm (C_4AH_{13} and C_2FH_8) and the ferrite residue CF_2H_x, formed due to reaction with water [1], or crystalline AFt formed according to reaction [3] or [5]. The two iron-rich phases, C_2FH_8 and CF_2H_x, have been observed in solutions with gypsum and $Ca(OH)_2/Ca_3SiO_5$, but they have also been observed (together with C_4AH_{13}) when ferrite is hydrated in pure water- where no retardation of the hydration is observed (3). Amorphous AFm (C_4AH_{13} and C_2FH_8) and the residual phase CF_2H_x can therefore not be responsible for the covering layer by themselves. Considering AFt, the actual needle shape of the crystals is evidence against it forming a compact covering layer, but it is clear that there are big differences in the shape of crystals formed in solutions with and without $Ca(OH)_2$ or Ca_3SiO_5. The presence of $Ca(OH)_2$ or Ca_3SiO_5 affects the crystal growth such that both AFt and AFm crystals become smaller and less well defined, cf Figs. 2(a)-(f). Also, the composition of AFt is modified when $Ca(OH)_2$ or Ca_3SiO_5 is present, the iron content being higher and the sulphate content lower. Pöllmann et al. (12) have observed that the differences in AFt crystal morphology could be connected to the substitution of sulphate by hydroxide or carbonate. If the covering layer during the dormant period is built up by AFt, it is possible that this substitution contributes to the forming of a more compact covering layer by making the crystals smaller and less well defined.

Considering the arguments presented above, we propose that the *combination* of small AFt crystals and X-ray amorphous phases is required in order to build up an effective covering layer, see Fig. 3. The AFt formation requires a lot of water, and AFt therefore acts as a drying agent in the amorphous layer. For effective drying to occur, the AFt crystals must be numerous, small and in good contact with the amorphous layer. As AFt forms, the X-ray

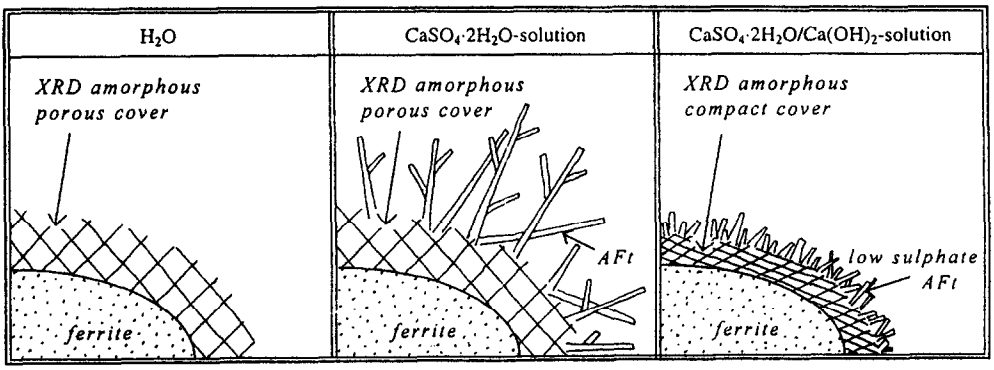

FIG. 3.
Schematic drawing illustrating the proposed model for the formation of a protective layer on the ferrite surface, leading to passivity. The formation of a non-porous surface layer requires the presence of an amorphous material in intimate contact with fine-grained AFt. Crystallization of AFt then desiccates the amorphous layer, which becomes compacted and water proof.

amorphous layer becomes dry and compact. To achieve the effect, the right mixture of X-ray amorphous phases and fine-grained AFt must form, e.g. C_4AH_{13}, C_2FH_8, CF_2H_x and $C_6A_{0.5}F_{0.5}\bar{S}_2H_{34}$ which are formed in gypsum + $Ca(OH)_2/Ca_3SiO_5$ solution. In gypsum solution, the AFt crystals are less numerous and bigger, which prevents effective drying. Consequently no retardation is achieved, just as in the case with pure water.

The notion that the products formed before and after the dormant period differ is supported by Figs. 2(a)-(d). Figs. 2(a) and (c) show AFt crystals formed in gypsum solution early and late during the AFt formation, respectively. The crystals show no difference in size and shape as expected, since no dormant period exists. Fig. 2(b) shows a mix of very small, platy and needle-like crystals, possibly the covering sheet, formed in gypsum + $Ca(OH)_2$ solution early during the dormant period. After the dormant period, cf Fig. 2(d), the crystals have the characteristic needle-like AFt shape, though smaller than the corresponding ones formed in gypsum solution. This has also been observed in samples with gypsum + Ca_3SiO_5 (4). The proposed model in Fig. 3 is also in general agreement with the in-situ TEM studies by Scrivener on hydrating C_3A and C_4AF (21).

Acknowledgment

The authors thank the Scancem Fund, Cementa AB and Scancem Research AB for supporting this project financially.

References

1. RILEM Committee 68-MMH, Task Group 3, Matér. Constr. 19, 137 (1986).
2. H.F.W. Taylor, Cement Chemistry, Academic Press, London (1990).
3. A. Emanuelson, E. Henderson and S. Hansen, Cem. Concr. Res. 26, 1689 (1996).
4. A. Emanuelson, S. Hansen, E. Henderson, A. Landa-Cánovas and E. Sjöstedt, 10th ICCC, 1i060 (1997).

5. S. Chatterji and J.W. Jeffery, J. Am. Ceram. Soc. 45, 536 (1962).
6. P.W. Brown, J. Am. Ceram. Soc. 70, 493 (1987).
7. E.T. Carlson, J. Res. Natl. Bur. Stand. 68A, 453 (1964).
8. M. Fukuhara, S. Goto, K. Asaga, M. Daimon, R. Kondo and Y. Ono, Yogyo Kyokaishi 88, 435 (1980).
9. T. Liang and Y. Nanru, Cem. Concr. Res. 24, 150 (1994).
10. Natl. Bur. Stand. (U.S.) Monogr. 25, 1628 (1979).
11. Y. Xi, China Building Materials Academy, Beijing, China, JCPDS-card no 41-1451 (1989).
12. H. Pöllmann, H.-J. Kuzel and R. Wenda, Neues Jahrb. Mineral. Abhandl. 160, 133 (1989).
13. H. McMurdie, H. et al., Powder Diffraction 2, 44 (1987).
14. M.H. Roberts, 5th ISCC 2, 104 (1969).
15. T. Scheller and H.-J. Kuzel, 6th ICCC 2, 217 (1976).
16. R. Fisher and H.-J. Kuzel, Cem. Concr. Res. 12, 517 (1982).
17. W. Dosch, H. Keller and H. zur Strassen, 5th ISCC 2, 72 (1969).
18. H.-J. Kuzel, Zem.-Kalk-Gips 21, 493 (1968).
19. H. E. Schwiete and T. Iwai, Zem.-Kalk-Gips 17, 379 (1964).
20. R. Buhlert and H.-J. Kuzel, Zem.-Kalk-Gips 24, 83 (1971).
21. K.L. Scrivener and P.L. Pratt, p. 207 in The Chemistry and Chemically-Related Properties of Cement (F.P. Glasser, Ed.) Brit. Ceram. Proc. no. 35 (1984).